CHAPTER 8

Global Morphometric Maps of Mars, Venus, and the Moon

Igor V. Florinsky

Institute of Mathematical Problems of Biology, Russian Academy of Sciences, Pushchino, Moscow Region, Russia

Abstract

The paper examines capabilities of digital terrain modelling to analyse topography of Mars, Venus, and the Moon at the global scale. Digital elevation models with a resolution of 30 arc-minutes were used as initial data. Fifteen local, regional, and combined topographic variables were for the first time calculated and mapped for the entire surface of the celestial bodies. In terms of geomorphological and geological interpretation, the most useful were maps of horizontal and vertical curvatures as well as catchment and dispersive areas. On catchment area maps of Mars and Venus, it was possible to detect several helical structures encircling the planets from pole to pole. Their origin may be connected with palaeorotational planetary stresses. A map of topographic index may be used to study the spatial distribution of the water ice deposits in the Martian soil.

Keywords: digital terrain modelling, surface, geology, planet

1 Introduction

Topography, resulting from endogenous and exogenous geophysical processes of various spatial and temporal scales, carries information both on these processes and target properties. This has led geoscientists to use morphometric analysis at different scales. At present, digital terrain modelling is the basis for investigations of this kind (Moore et al. 1991; Florinsky 1998a; Wilson and Gallant 2000).

Digital terrain models (DTMs) are widely used in research of the planets of the Earth group, satellites, and asteroids, including refinements of the shape of a celestial body (Sadovnichy et al. 1991; Smith et al. 1997; Nyrtsov 2000), studies of the global and regional tectonic structures (Solomon et al. 1991; Zuber et al. 1994; Watters et al. 2001; Nimmo et al. 2003), prediction of the crust structure (Zuber et al. 2000; Wieczorek 2007), modelling of lithospheric evolution (Smith et al. 1999; Byrne 2007) and mantle convection (Simons et al. 1994), statistical characterisation of the relief (Lucey et al. 1994; Barnouin-Jha et al. 2008), geomorphic mapping (Bue and Stepinski 2006), studies of volcanic (Neukum et al. 2004), glaciological (Fishbaugh and Head 2001; Neukum et al. 2004), and erosional processes (Williams et al. 2005), modelling of impact structures (Cochrane and Ghail 2006), reconstruction of palaeohydrological events (Carr and Head 2003) and palaeoclimatic conditions (Stepinski and Stepinski 2005), valley network detection (Jenson 1991; Molloy and Stepinski 2007), and selection of landing sites (Kirk et al. 2003).

Local topographic variables of the complete system of curvatures (Shary 1995) and regional topographic variables (Speight 1974) are key parameters of geomorphometry. However, they have not been used in planetary studies at the global scale. A recent analysis of the Earth's global topography demonstrated the usefulness of these attributes (Florinsky 2008). This paper examines capabilities of digital terrain modelling to analyse the global topography of Mars, Venus, and the Moon.

2 Materials and Methods

The study was based on 30 arc-minute gridded global digital elevation models (DEMs) of Mars, Venus, and the Moon. A DEM of Mars (Fig. 8.1a) was obtained from the Mars Orbiter Laser Altimeter Mission Experiment Gridded Data Record (MOLA MEGDR) archive (Smith 2003) of the Mars Global Surveyor mission (Albee 2000). A DEM of Venus (Fig. 8.1b) was compiled using data from two archives of the Magellan mission

(Saunders and Pettengill 1991), viz. Global Topography Data Record (GTDR) (Ford 1992) and Magellan Spherical Harmonic Models and Digital Maps (MSHMDM) (Sjogren 1997). A DEM of the Moon (Fig. 8.1c) was extracted from the Clementine Gravity and Topography Data (CGTD) archive (Zuber 1996) of the Clementine mission (Nozette et al. 1994).

Each DEM included 260,281 points (721 by 361 matrices). Martian and Lunar elevations were presented with reference to related geoids (Zuber et al. 1994; Smith et al. 1999), while Venusian ones – with reference to the mean planetary radius (Rappaport et al. 1999).

Any DEM includes high frequency noise leading to the derivation of useless, noisy digital models and unreadable maps of topographic variables (Florinsky 2002). The problem can be partially resolved by DEM smoothing. One, two, and three smoothing iterations were applied to the DEMs using a 3 by 3 kernel with linear inverse distance weights.

For Mars, Venus, and the Moon, digital models of fifteen topographic attributes were derived: twelve local variables (i.e., horizontal, vertical, accumulation, difference, ring, minimal, maximal, mean, Gaussian, unsphericity, horizontal excess, and vertical excess curvatures), two regional variables (i.e., catchment and dispersive areas), and a combined variable, topographic index (*TI*). Definitions, formulae, and interpretations of the variables can be found elsewhere (Florinsky 1998a; Shary et al. 2002).

The method designed for a spheroidal trapezoidal grid (Florinsky 1998b) was applied to calculate local variables. A spheroidal trapezoidal moving window was used in calculations. Its linear sizes depend on the latitude. Known formulae for the inverse geodetic problem (Vincenty 1975; Morozov 1979, pp 178–179) were employed to estimate window sizes during calculations (Florinsky 1998b, 2008). These formulae were also applied to estimate window sizes and point weights during DEM smoothing.

Calculation of regional variables from a DEM is based on logistic procedures, such as cell-to-cell flow line routing. These variables were derived by a single flow line direction algorithm with preliminary filling of sinks (Martz and de Jong 1988) adapted for a spheroidal trapezoidal grid. In a given pixel, a catchment area equals a total area of pixels passed by flow lines arriving the given pixel. An elementary spheroidal trapezoidal area depends on the latitude; it can be estimated by the known formula (Morozov 1979, p 34).

TI is a function of slope steepness and catchment area, that is, local and regional variable, correspondingly. Hence, for an spheroidal trapezoidal DEM, *TI* calculation is based on both of approaches described above.

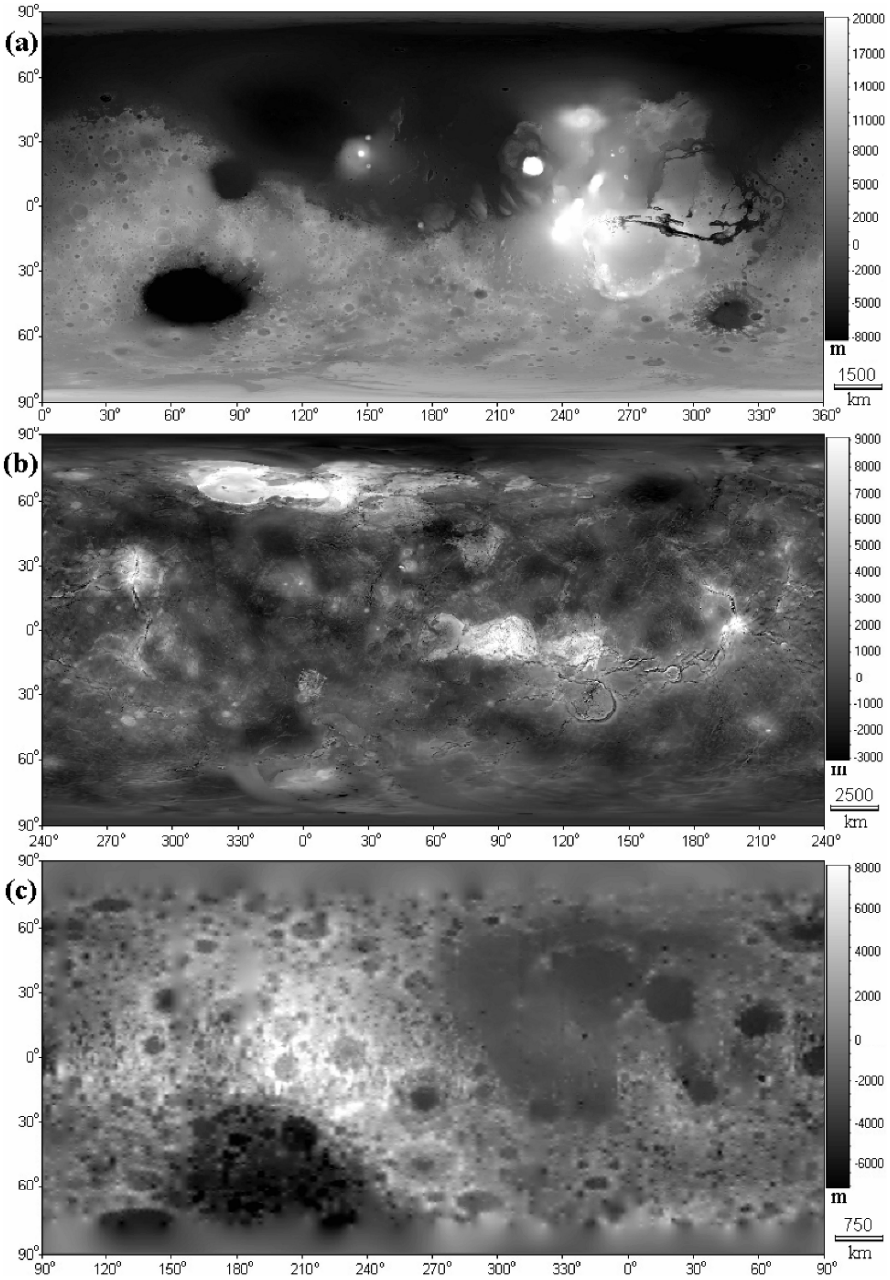

Fig. 8.1. Elevation: (a) Mars, (b) Venus, and (c) the Moon

To estimate linear sizes of an spheroidal trapezoidal window, standard values of the major and minor semiaxes of the Martian ellipsoid were

used: 3,396,190 and 3,376,200 m, correspondingly (Seidelmann et al., 2002). Venus and the Moon were considered as spheres of 6,051,848 and 1,738,000 m radii, correspondingly. The DEMs were processed as virtually closed spheroidal matrices. DTMs were derived from smoothed DEMs. DTMs had the resolution of 30 arc-minutes consisting of 721 columns by 361 rows.

It is undesirable to map a topographic variable with an equal-step quantification of its values. This usually leads to information loss due to the large dynamic range of a digital model. To gain a better representation and understanding of global morphometric maps, DTMs were logarithmically transformed as follows (Eq. 8.1):

$$\Theta' = \mathrm{sign}(\Theta) \cdot \ln(1 + 10^n |\Theta|), \tag{8.1}$$

where Θ represents a topographic variable, $n = 0$ for regional variables, $n = 16$ for accumulation, ring, and Gaussian curvatures, and $n = 9$ for other attributes (Figs. 8.2–8.5)

This sort of transformation (Shary et al. 2002) allows one to hold ranges of positive and negative values of a variable (Figs. 8.2–8.3). *TI* was not transformed as its formula includes logarithm calculation. Catchment and dispersive areas were also mapped classifying their values into two levels (Fig. 8.7). The Plate Carrée projection was used to map all variables (Figs. 8.1–8.7). DTM treatment was carried out with LandLord 4.0 (Florinsky et al. 1995).

3 Results and Discussion

3.1 General Geomorphometric Interpretation

Global maps of topographic variables represent peculiarities of the megarelief of Mars, Venus, and the Moon in different ways, according to the physical and mathematical sense of a particular variable.

Horizontal curvature (Fig. 8.2) delineates areas of divergence and convergence of slope lines (positive and negative values, respectively) (Florinsky 1998a; Shary et al. 2002). These areas correspond to valley and ridge spurs (dark and light patterns, respectively), which form so-called flow structures.

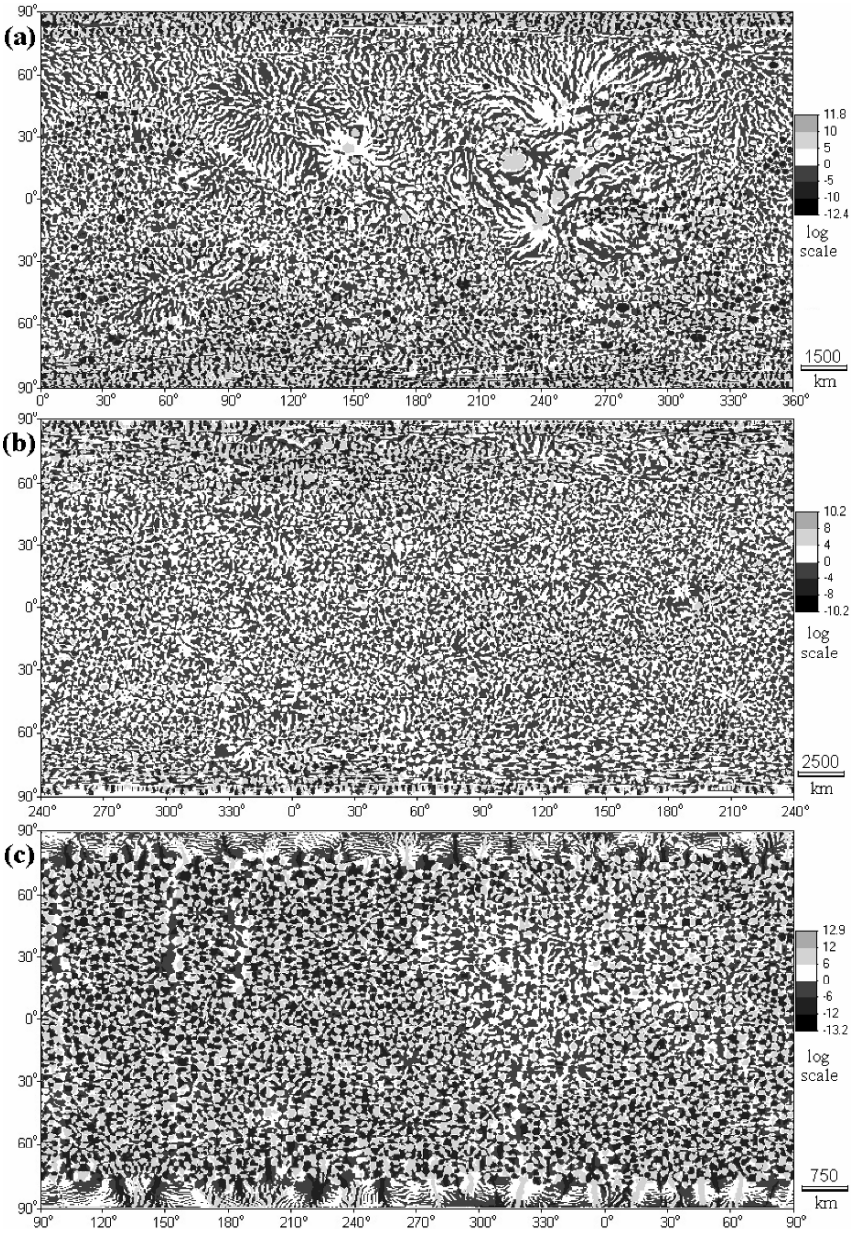

Fig. 8.2. Horizontal curvature derived from the 2-times smoothed DEMs: (a) Mars, (b) Venus, and (c) the Moon

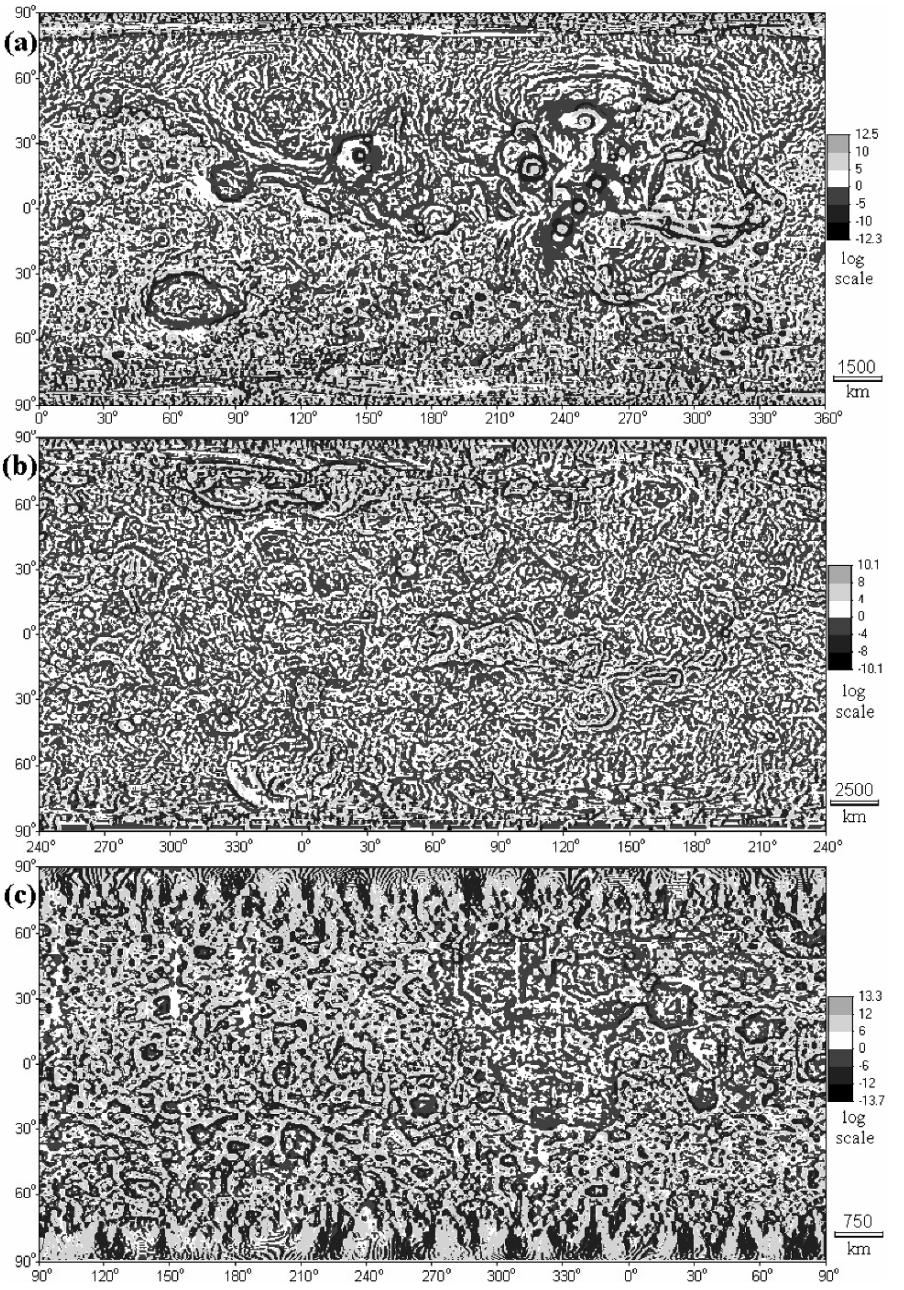

Fig. 8.3. Vertical curvature derived from the 2-times smoothed DEMs: (a) Mars, (b) Venus, and (c) the Moon

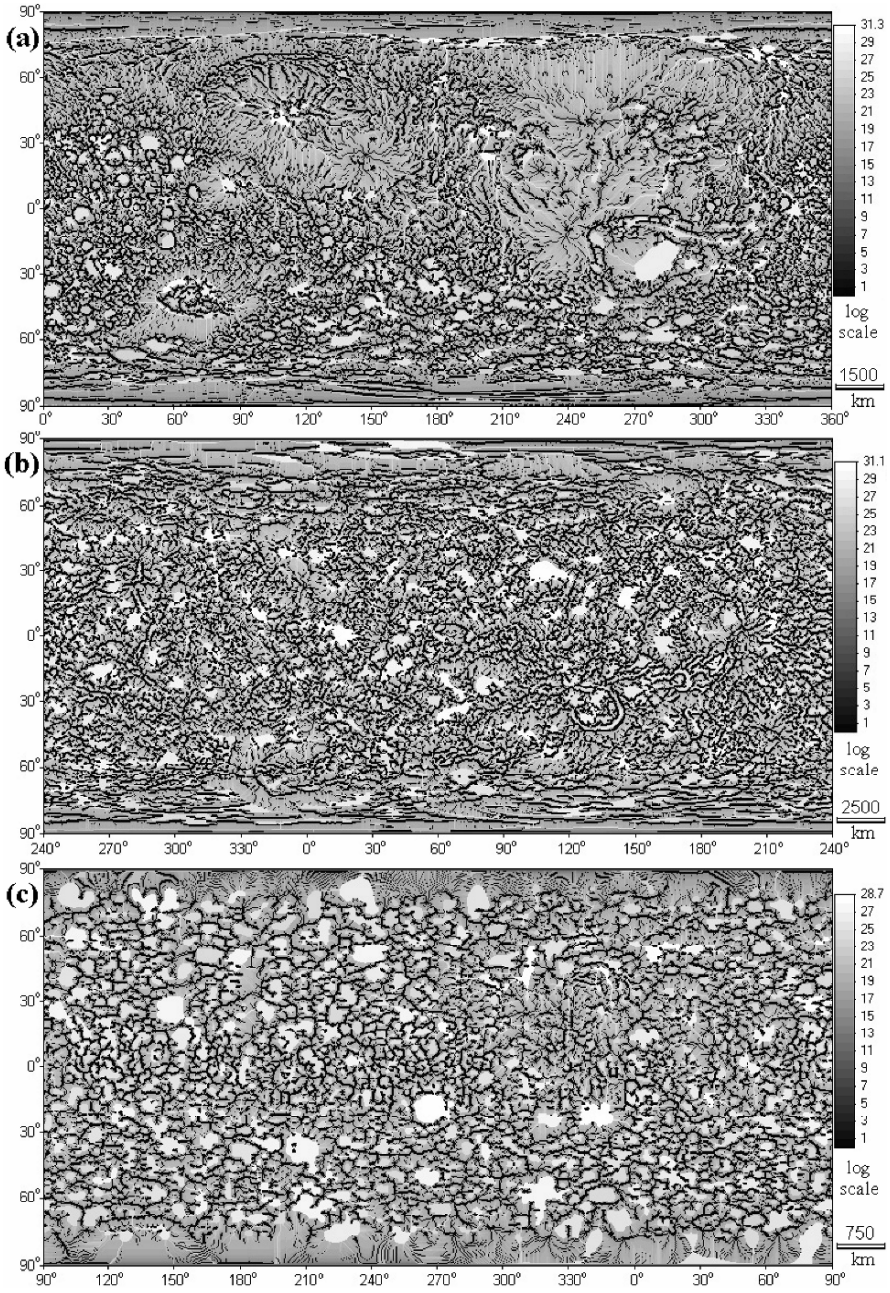

Fig. 8.4. Catchment area derived from the 1-time smoothed DEMs: (a) Mars, (b) Venus, and (c) the Moon

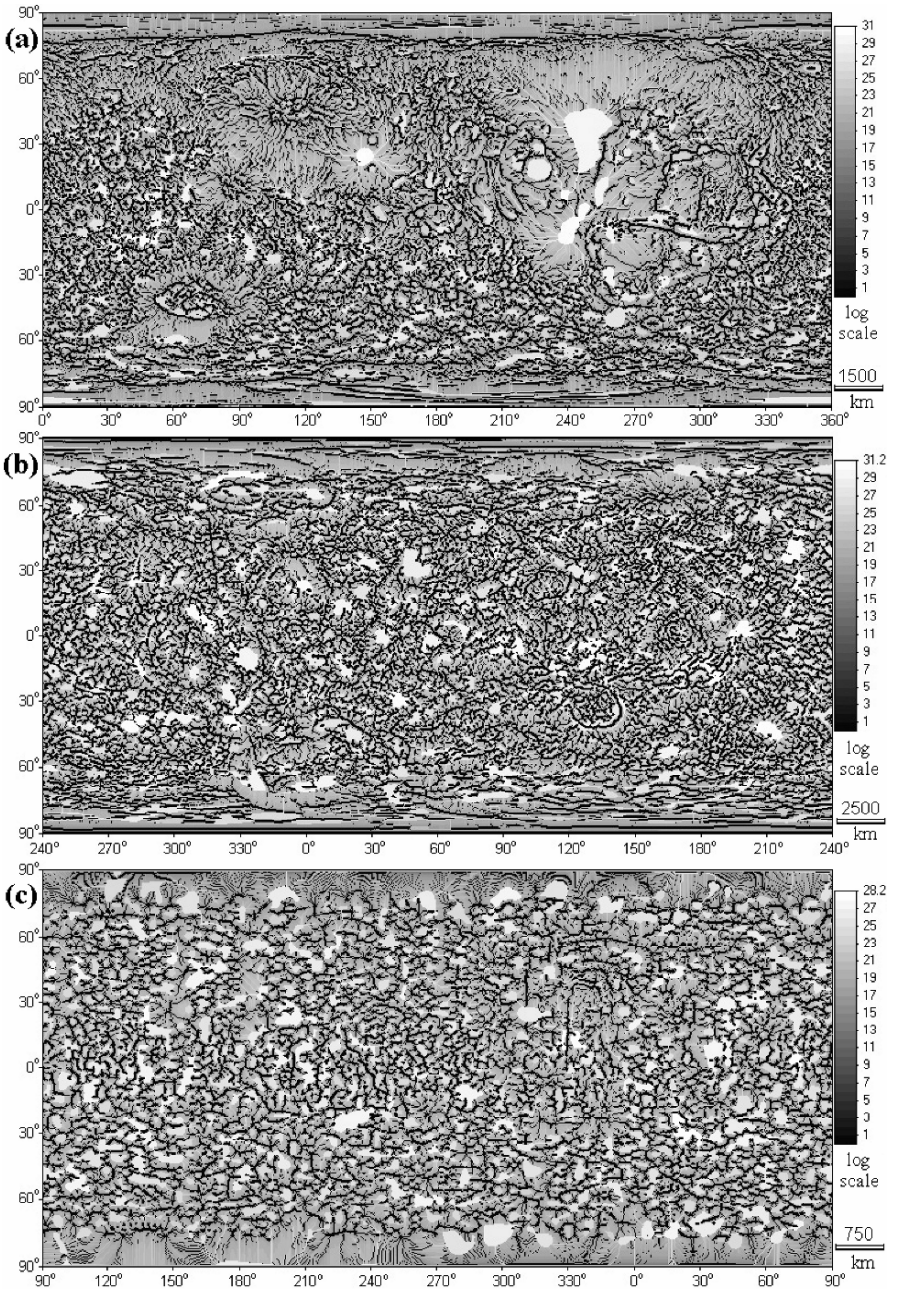

Fig. 8.5. Dispersive area derived from the 1-time smoothed DEMs: (a) Mars, (b) Venus, and (c) the Moon

At the global scale, flow structures are most pronounced on Mars (Fig. 8.2a). In particular, one can see flow structures, probably, of lava origin, beginning on slopes of Alba Patera and forming a huge fan in North Polar Basin (30°–75°N, 200°–310°E). There is a system of flow structures incoming to Utopia Planitia from Nilosyrtis and Protonilus Mensae and Elysium Planitia and Mons (5°–70°N, 75°–150°E). On Venus, flow structures appear only slightly at the global scale (Fig. 8.2b). One can see them on the slopes of Beta Regio (15°–45°N, 270°–300°E). For the Moon, the horizontal curvature represents cellular-like patterns (Fig. 8.2c) resulted from a predominance of craters at the global scale.

Vertical curvature (Fig. 8.3) is a measure of relative acceleration and deceleration of slope lines (positive and negative values, respectively) (Florinsky 1998a; Shary et al. 2002). At the global scale, vertical curvature maps show 'mega-scarps', such as edges of plains, basins, and mountains. For example, on the vertical curvature map of Mars (Fig. 8.3a), one can see borders of Hellas Planitia (30°–50°S, 50°–90°E), Isidis Planitia (10°–25°N, 75°–100°E), Valles Marineris (10°–20°S, 270°–335°E), foothills of Olympus Mons (15°–20°N, 220°–230°E), Alba Patera (30°–50°N, 225°–265°E), etc. Artemis Chasma (30°–45°S, 120°–145°E) and some other surface features are pronounced on the vertical curvature map of Venus (Fig. 8.3b). On the vertical curvature map of the Moon (Fig. 8.3c), one can see well-marked borders of Mare Serenitatis (15°–40°N, 10°–30°E), Mare Crisium (10°–20°N, 50°–70°E), etc.

Catchment area measures an upslope area potentially drained through a given point on the surface (Florinsky 1998a; Shary et al. 2002). At the global scale, low values of the catchment area (Fig. 8.4) delineate ridges as black lines, while its high values show valleys as white lines and depressions as light areas. On the catchment area map of Mars (Fig. 8.4a), one can see the planetary network of valleys and canyons. A large feature, Solis Planum (15°–30°S, 270°–290°E), and a plethora of smaller depressions, predominantly craters, stand out. On the catchment area map of the Moon (Fig. 8.4c), one can see borders of Mare Orientalis (15°–25°S, 255°–275°E), Mare Nubium (20°–25°S, 340°–350°E), etc.

Dispersive area measures a downslope area potentially exposed by slope lines passing through a given point on the surface (Shary et al. 2002). At the global scale, high values of the dispersive area delineate mountains and highlands as light areas (Fig. 8.5). For example, the planetary network of ridges can be observed on the dispersive area map of Mars (Fig. 8.5a). Alba Patera (30°–50°N, 230°–260°E), Tharsis Montes (15°N–15°S, 230°–260°E), and other surface features stand out.

On all maps, recognisable artefacts are typical for polar regions (Figs. 8.2–8.7). They were caused by a relatively low accuracy of description of

these areas in the databases used (MOLA MEGDR, GTDR, MSHMDM, and CGTD). Besides, CGTD systematic errors led to several meridian artefacts, such as stripes up to 5° wide (80°S–80°N, 155°E; 10°–60°N, 185°E; etc.), on Lunar maps of elevation, horizontal and vertical curvatures, and dispersive area (Figs. 8.1c, 8.2c, 8.3c, and 8.5c). The Venusian DEM was compiled combining data from GTDR and MSHMDM. These archives are marked by distinct resolution and accuracy. As a result, one can see several linear artefacts – marks of this combination (e.g., 15°–55°N, 325°E; 60°–80°S, 325°–355°E) on Venusian maps of elevation, vertical curvature, and catchment and dispersive areas (Figs. 8.1b, 8.3b, 8.4b, and 8.5b).

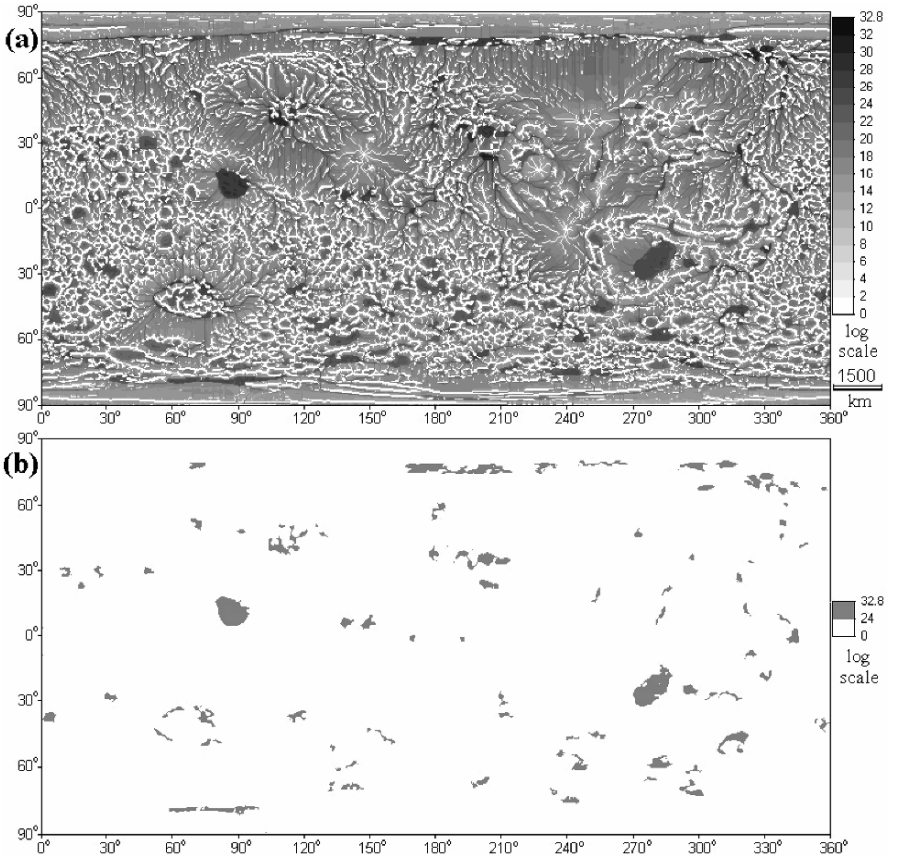

Fig. 8.6. Mars, topographic index: (a) general map, and (b) *TI* values quantified into two levels

There are also computational artefacts on maps of catchment and dispersive areas manifested as straight parallel lines predominantly in polar

regions (Figs. 8.4 and 8.5). They are well known artefacts of single flow line direction algorithms common for flat slopes (e.g., Liang and Mackay 2000). However, the artefacts did not influence the perception of topographic features since the artefacts are situated within limited zones of the maps.

3.2 Spatial Distribution of the Water Ice on Mars

One of the topical problems of Mars studies is the elucidation of the spatial distribution of the subsurface water ice (Baker 2001; Cabrol and Grin 2005; Kuzmin 2005; Mitrofanov 2005; Bandfield 2007). It is supposed that water ice (e.g., frozen groundwater, frozen and dust-covered lakes) may be located in the soil to a depth of 1–2 m (Boynton et al. 2002; Mitrofanov 2005; Bandfield 2007). There are several global models for the spatial distribution of the subsurface water ice, particularly based on the neutron spectrometer data (Mitrofanov 2005). It was noted that the Martian topography might theoretically control the spatial distribution of liquid water on the surface: atmospheric pressure exceeds a value critical for the existence of liquid water in some deep depressions (Tokano 2005).

In hydrological studies, *TI* is used to model and predict the spatial distribution of soil moisture and depth to the saturation zone (Beven and Kirkby 1979; Quinn et al. 1995). High values of *TI* are typical for flat territories draining large upslope areas. The higher *TI* value, the higher a soil moisture content, and the less a depth to the saturation zone.

Is it possible to use the global *TI* map of Mars (Fig. 8.6a) to predict the spatial distribution of subsurface water ice? To do this would require, at least, three assumptions. First, at the global scale, relief has varied only slightly after the finish of active tectonic processes responsible for the latest large hydrological events on Mars, such as glacier melting and catastrophic flooding (Baker 2001). Relief changes due to exogenous (e.g., erosion and aeolian) processes can be ignored at this scale. Second, soil water, groundwaters, and lakes turned from liquid into solid state on completion of active tectonic processes and, since that time, ice was preserved intact. Three, there is no ground ice derived from the atmosphere.

If one may accept these assumptions, than *TI* map (Fig. 8.6a) may display the spatial distribution of subsurface water ice. The higher values of *TI* (the darker patterns), the higher an ice content in the soil and the less a depth of ‘the ice table’. Quantifying *TI* values into two levels (Fig. 8.6b), one can delineate regions where relief properties have formed prerequisites for the largest deposits of the subsurface ice. Among these are Solis Planum (15°–30°S, 270°–290°E), Isidis Planitia (5°–20°N, 75°–100°E),

several zones at Amazonis Planitia (20°–40°N, 175°–215°E) and Utopia Planitia (40°–50°N, 105°–130°E).

It should be stressed that patterns of the *TI*-based prediction of the ground ice distribution differ essentially from those based on other data and models (Boynton et al. 2002; Kuzmin 2005). A further research (e.g., a comparative analysis of remotely sensed (Bandfield 2007) and *TI* data), should demonstrate if *TI* mapping was selected adequately to predict the spatial distribution of subsurface water ice on Mars.

3.3 Global Helical Structures

Classification of catchment area values into two levels allows one to display ridge networks of Mars (Fig. 8.7a), Venus (Fig. 8.7b), and the Moon (Fig. 8.7c). Analysing of the similar binary maps of the Earth, the author revealed five systems of double helical-like tectonic structures encircling the planet from pole to pole (Fig. 8.8). The structures are topographically expressed by patterns of the global ridge network. They are apparently associated with traces of palaeorotational planetary stresses: two double helices are in reasonable agreement with theoretically predicted traces of shear fractures, while another two double helices are in reasonable agreement with ideal traces of cleavage cracks. Various geological phenomena, such as fracturing, faults, as well as crystal and ore deposits are observed along the helical structures (Florinsky 2008).

Question arises: are global helical structures unique for the Earth, or similar features may be observed on other planets of the Earth group and satellites? The catchment area maps of the celestial bodies (Fig. 8.7) were examined in detail. Attention was paid to lineaments running over the entire globe or a hemisphere. Contrary to regional and continental lineaments, global ones are not manifested as uninterrupted linear patterns or their sequences. A global lineament may be visually detected due to traits of the image texture strung out along a line of some direction (Florinsky 2008).

The visual analysis allowed the author to delineate several global lineaments on Mars and Venus (Fig. 8.9). The global helical structures encircle the planets from pole to pole. The structures revealed are obviously helical zones rather than simply lines. Each helical zone transgresses regions dissimilar in respect to their geomorphic and geological composition.

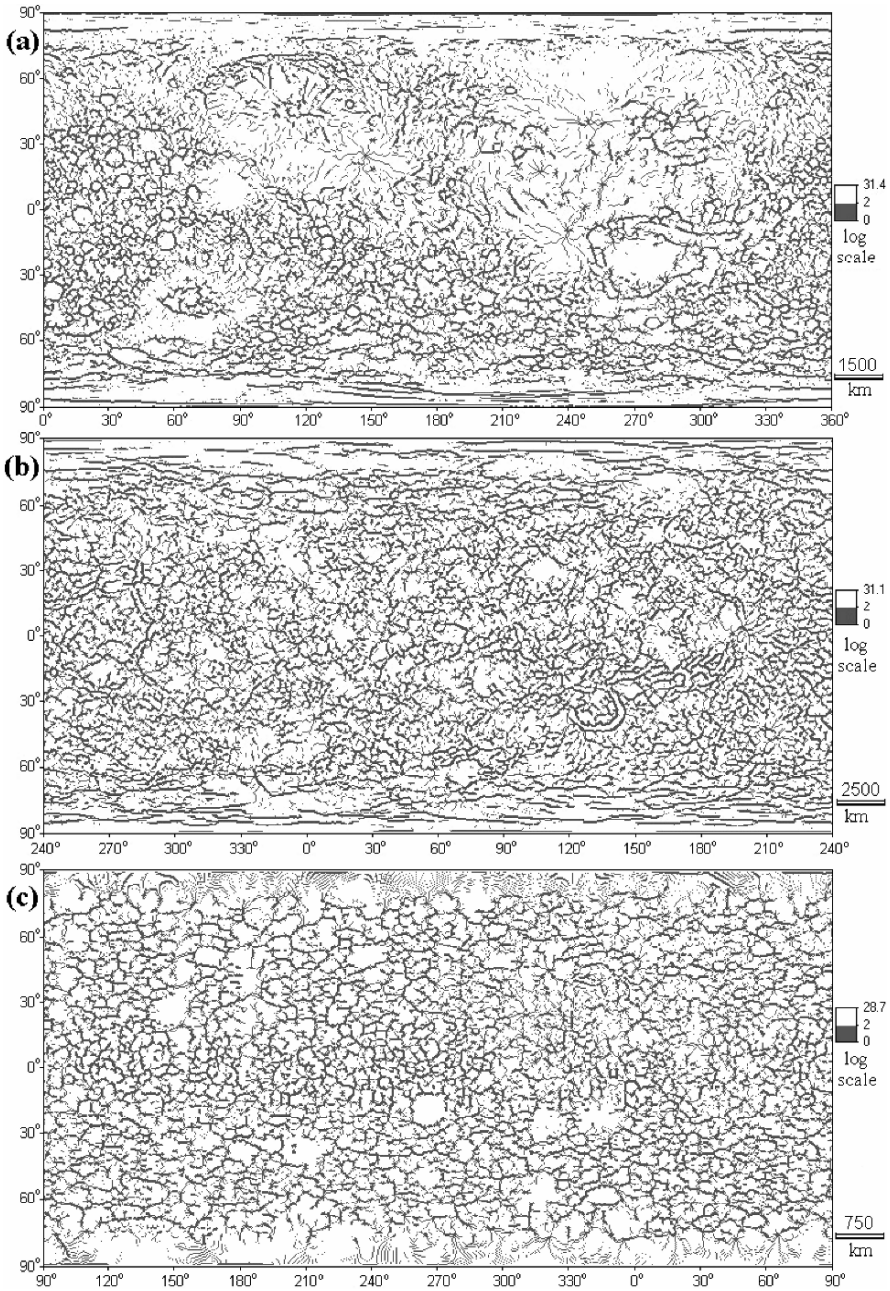

Fig. 8.7. Binary maps of the catchment area: (a) Mars, (b) Venus, and (c) the Moon. Maps of Mars and Venus were derived from the 2-times smoothed DEMs; the Moon map was derived from the 1-time smoothed DEM

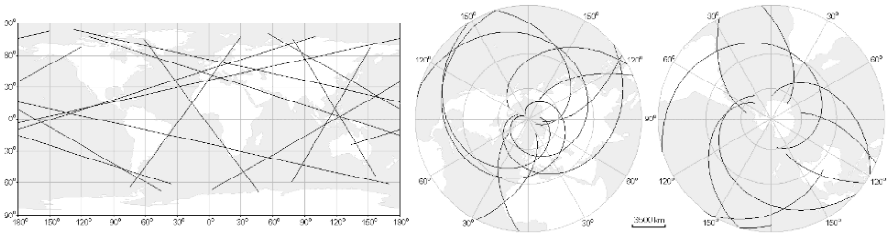

Fig. 8.8. Global helical structures of the Earth; the Plate Carrée projection (left), and polar stereographic projections for the Northern (centre) and Southern (right) hemispheres (Florinsky 2008)

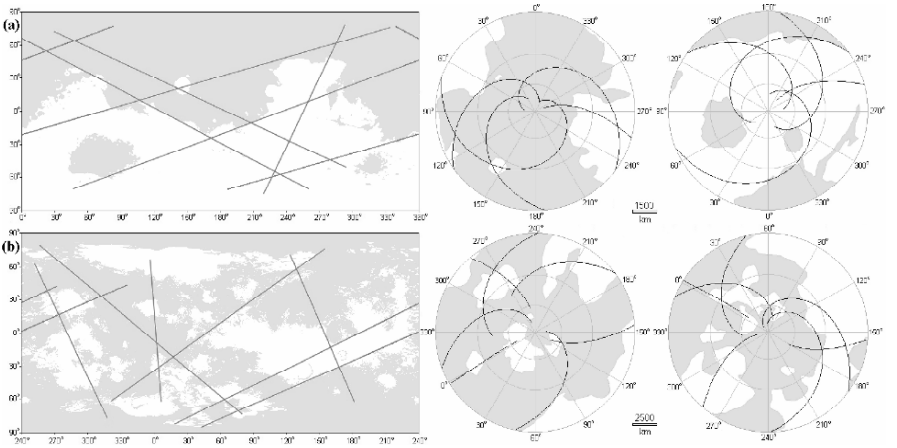

Fig. 8.9. Global helical structures: (a) Mars, and (b) Venus; the Plate Carrée projection (left), and polar stereographic projections for the Northern (centre) and Southern (right) hemispheres. Grey colour indicates areas located below datum

The global lineaments revealed cannot be artefacts due to DEM errors, DEM treatment, or DEM grid geometry (Florinsky 2005). First, noise and errors usually have a random distribution in DEMs. Second, smoothing and derivation of topographic variables were carried out using local filters (*n* by *n* moving windows). Third, the grid geometry may amplify its own preferential directions: orthogonal (north-south, east-west) and diagonal (northeast-southwest, northwest-southeast). However, the structures detected have (a) the global character relative to the DEMs, and (b) directions distinct from orthogonal and diagonal ones (Fig. 8.9).

Thus, possible artefacts may be caused by a subjectivity of the visual analysis only. One may speculate that some automated tools (Fukue et al. 1981; Takahashi 1981; Zlatopolsky 1992) should be used to reveal lineaments rather than the visual analysis. However, experiments demonstrated

that an ideal observer (Swets 1961) and the human visual system are marked by almost similar possibilities to recognise geometrical patterns on noisy binary images (Krasilnikov et al. 2000). Therefore, it is questionable whether an application of an automated tool could reveal radically different lineaments. In the past, numerous geological studies have also demonstrated that visual analysis of maps and remotely sensed data can be successfully used to detect lineaments (Hobbs 1904; Lattman 1958; Shults 1970; O'Leary et al 1976; Makarov 1981; Trifonov et al 1983).

There is circumstantial evidence that global helical structures (Fig. 8.9) are not artefacts. First, some spiral structures have been documented for the Martian polar caps (Howard 1978, 2000; Fishbaugh and Head 2001). These are troughs and scarps 5–30 km wide and up to several hundreds kilometres long. Trough depths are up to 500–1000 m on polar caps edges, and 100–200 m near poles. Martian polar spiral structures are usually considered as an overall result of ice elastic deformations and sublimation influenced by katabatic wind flows, which are affected by Coriolis forces (Howard 1978, 2000; Weijermars 1985/86; Fisher 1993).

Second, Slyuta et al. (1989) discovered a dense, regular network of dextral and sinistral spiral structures on radar scenes of the Northern hemisphere of Venus. These planetary structures are wound around the axis of rotation of Venus. They are topographically manifested as troughs, scarps, and depressions. Slyuta et al. (1989) believed that strong rotational forces had formed the network during the deceleration of Venus's rotation. They suggested that the helical network is a relict feature, 'imprint' of ancient rotational stress fields, because the current rotation velocity of Venus is quite slow. The low intensity of erosion has allowed relict helical structures to persist on the Venusian surface.

The author supposes that origin of global helical structures of Mars and Venus (Fig. 8.9) may be connected with palaeorotational planetary stresses. Detailed analysis of global helices of Mars and Venus is the objective of further studies.

It is notable that global lineaments were not found on the catchment area map of the Moon (Fig. 8.7c). This may be connected with peculiarities of the rotational regime of the satellite. There is a hypothesis that a tectonic structure of a celestial body is generally controlled by parameters of its orbit(s) (Kochemasov 1999). Unlike planets having one orbit, satellites have two orbits. This increases a complexity or heterogeneity of a tectonic structure of a satellite as compared to a planet (Kochemasov 2006). The lack of topographically manifested helical structures on the Moon may be explained by this proposal (Kochemasov 2008, personal communication).

4 Conclusions

The paper examines capabilities of digital terrain modelling to analyse global topography of Mars, Venus, and the Moon. For the celestial bodies, global digital models and maps of fifteen local, regional, and combined topographic variables were derived. Global maps of topographic variables represented peculiarities of the relief in different ways, according to the physical and mathematical sense of a particular variable. A preliminary analysis demonstrated that the most useful were maps of horizontal and vertical curvatures as well as catchment and dispersive areas. The horizontal curvature revealed flow structures, while the vertical curvature detected mega-scarps. Mapping of the catchment and dispersive areas delineated global networks of ridges and valleys. On binary maps of the catchment area, it was possible to detect several helical structures encircling Mars and Venus from pole to pole. Detailed interpretation of the tectonic helices is the objective of a further research. *TI* map may be used to study the spatial distribution of the water ice in the Martian soil.

Relatively low accuracy of the initial data for Venus and the Moon limited the detection of topographic structures and interpretation of the morphometric maps. Considering current trends in the Solar system investigation, in the medium-term future one would expect the production of new global DEMs of Venus, the Moon, and other celestial bodies (Haruyama et al. 2008), which accuracy would be comparable with the DEM of Mars.

The existed geological maps of Mars, Venus, and the Moon (U.S. Geological Survey 1972; Scott and Carr 1978; Ivanov 2008) can be integrated with the maps of topographic variables. They may be useful in solving various tasks of planetary science: to refine borders of topographic and geological structures, to describe them quantitatively, to analyse their spatial distribution over the planetary surface, etc. The use of digital terrain modelling in planetary studies can tangibly improve our knowledge about planets, satellites, and asteroids.

Acknowledgments

The author thanks GG Dikevich (Moscow, Russia), VF Pankin (Cartgeocentre, Moscow, Russia), RL Kirk (Astrogeology Team, USGS, Flagstaff, USA), AE Fedorov (Annual Seminar ‘The System of the Planet Earth: Non-Conventional Problems of Geology’, Moscow, Russia), GG Kochemasov (Institute of Ore Deposit Geology, Petrography, Mineralogy and

Geochemistry, Russian Academy of Sciences, Moscow, Russia), and three anonymous referees for suggestions, as well as S Slavney (PDS Geosciences Node, Washington University, St. Louis, USA), VG Karpova, EK Vershinina (Lundbeck, Kiev, Ukraine), and TE Petrova (Institute of Mathematical Problems of Biology, Russian Academy of Sciences, Pushchino, Russia) for assistance.

References

Albee AL (2000) Mars 2000. Ann Rev Earth Plan Sci 28:281–304

Baker VR (2001) Water and the Martian landscape. Nature 412:228–236

Bandfield JL (2007) High-resolution subsurface water-ice distributions on Mars. Nature 447:64–67

Barnouin-Jha OS, Cheng AF, Gaskell RW (2008) The surface roughness of asteroid 25143 Itokawa and 433 Eros. In: Abstracts of the 39th Lunar planetary Science Conference, 10–14 March 2008. League City, Texas, # 1297

Beven KJ, Kirkby MJ (1979) A physically-based variable contributing area model of basin hydrology. Hydrol Sci Bull 24:43–69

Boynton WV, Feldman WC, Squyres SW, Prettyman T, Brückner J, Evans LG, Reedy RC, Starr R, Arnold JR, Drake DM, Englert PAJ, Metzger AE, Mitrofanov I, Trombka JI., d'Uston C, Wänke H, Gasnault O, Hamara DK, Janes DM, Marcialis RL, Maurice S, Mikheeva I, Taylor GJ, Tokar R, Shinohara C (2002) Distribution of hydrogen in the near-surface of Mars: evidence for sub-surface ice deposits. Science 297:81–85

Bue BD, Stepinski TF (2006) Automated classification of landforms on Mars. Comp Geosci 32:604–614

Byrne CJ (2007) A large basin on the near side of the Moon. Earth Moon Planets 101:153–188

Cabrol NA, Grin EA (2005) Ancient and recent lakes on Mars. In: Tokano T (ed) Water on Mars and life. Springer, Berlin, pp 235–259

Carr MH, Head III JW (2003) Oceans on Mars: An assessment of the observational evidence and possible fate. J Geophys Res E108:5042

Cochrane CG, Ghail RC (2006) Topographic constraints on impact crater morphology on Venus from high-resolution stereo synthetic aperture radar digital elevation models. J Geophys Res 111:E04007

Fishbaugh KE, Head III JW (2001) Comparison of the north and south polar caps of Mars: new observations from MOLA data and discussion of some outstanding questions. Icarus 154:145–161

Fisher D (1993) If Martian ice caps flow: ablation mechanisms and appearance. Icarus 105:501–511

Florinsky IV (1998a) Combined analysis of digital terrain models and remotely sensed data in landscape investigations. Progr Phys Geogr 22:33–60

Florinsky IV (1998b) Derivation of topographic variables from a digital elevation model given by a spheroidal trapezoidal grid. Int J Geogr Inf Sci 12:829–852

Florinsky IV (2002) Errors of signal processing in digital terrain modelling. Int J Geogr Inf Sci 16:475–501

Florinsky IV (2005) Artificial lineaments in digital terrain modelling: can operators of topographic variables cause them? Math Geol 37:357–372

Florinsky IV (2008) Global lineaments: application of digital terrain modelling. In: Zhou Q, Lees B, Tang G-a (eds) Advances in digital terrain analysis. Springer, Berlin, pp 365–382

Florinsky IV, Grokhlina TI, Mikhailova NL (1995) LANDLORD 2.0: the software for analysis and mapping of geometrical characteristics of relief (in Russian). Geod Cartogr 5:46–51

Ford PG (1992) Magellan global topography, emissivity, reflectivity, and slope data, MGN-V-RDRS-5-GDR-TOPOGRAPHIC-V1.0, MGN-V-RDRS-5-GDR-EMISSIVITY-V1.0, MGN-V-RDRS-5-GDR-REFLECTIVITY-V1.0, and MGN-V-RDRS-5-GDR-SLOPE-V1.0, NASA planetary data system, http://pds-geosciences.wustl.edu/missions/magellan/gxdr/index.htm

Fukue K, Shimoda H, Sakata T (1981) Complete lineament extraction with the aid of shadow-free Landsat image. In: Machine processing of remotely sensed data with special emphasis on range, forest, and wetlands assessment. Proc 7th Int Symp, 23-26 June, 1981. Purdue University, West Lafayette, pp 94–102.

Haruyama J, Ohtake M, Matunaga T, Morota T, Honda C, Torii M, Yokota Y, Ogawa Y, Abe M, Hara S, Hioki K, LISM working group (2008) Kaguya (Selene) / Terrain Camera initial results and perspectives. In: Abstr 37th Lunar planetary sci conf, 13–17 March 2006, League City, Texas, # 1132

Hobbs WH (1904) Lineaments of Atlantic Border region. Geol Soc Amer Bull 15:483–506

Howard AD (1978) Origin of the stepped topography of the Martian poles. Icarus 34:581–599

Howard AD (2000) The role of Eolian processes in forming surface features of the martian polar layered deposits. Icarus 144:267–288

Ivanov MA (2008) Global geological map of Venus: preliminary results. In: Abstr 39th Lunar planetary sci conf, 10–14 March 2008, League City, Texas, # 1017

Jenson SK (1991) Applications of hydrologic information automatically extracted from digital elevation models. Hydrol Proc 5:31–44.

Kirk RL, Howington-Kraus E, Redding B, Galuszka D, Hare TM, Archinal BA, Soderblom LA, Barrett JM (2003) High-resolution topomapping of candidate MER landing sites with Mars Orbiter Camera narrow-angle images. J Geophys Res 108:8088

Kochemasov GG (1999) Theorems of wave planetary tectonics. Geophys Res Abstr 1:700

Kochemasov GG (2006) Anomalous parts on the Lunar crater size – frequency curve, their prediction and comparison of the Lunar and Solar discs granulation patterns. In: Abstr 36th COSPAR Sci Assembly, 16–23 July 2006, Beijing, China. CD-ROM, # 793

Krasilnikov NN, Krasilnikova OI, Shelepin YE (2000) Perception of achromatic, monochromatic, pure chromatic, and chromatic noisy images by real human-observer under threshold conditions. Proc SPIE 3981:78–85.

Kuzmin RO (2005) Ground ice in the Martian regolith. In: Tokano T (ed) Water on Mars and life. Springer, Berlin, pp 155–189

Lattman LH (1958) Technique of mapping geologic fracture traces and lineaments on aerial photographs. Photogram Eng 24:568–576

Liang C, Mackay DS (2000) A general model of watershed extraction and representation using globally optimal flow paths and up-slope contributing areas. Int J Geogr Inf Sci 14:337–358.

Lucey P, Spudis PD, Zuber M, Smith D, Malaret E (1994) Topographic-compositional units on the Moon and the early evolution of the lunar crust. Science 266:1855–1858

Makarov VI (1981) Lineaments: problems and trends of studies by remote sensing techniques (in Russian). Izv Vuz, Geol Razv, 4:109–115

Martz LW, de Jong E (1988) CATCH: a Fortran program for measuring catchment area from digital elevation models. Comp Geosci 14:627–640

Mitrofanov IG (2005) Global distribution of subsurface water measured by Mars Odyssey. In: Tokano T (ed) Water on Mars and life. Springer, Berlin, pp 99–128

Molloy I, Stepinski TF (2007) Automatic mapping of valley networks on Mars. Comp Geosci 33:728–738

Moore ID, Grayson RB, Ladson AR (1991) Digital terrain modelling: a review of hydrological, geomorphological and biological applications. Hydrol Proc 5:3–30

Morozov VP (1979) A course in spheroidal geodesy. 2nd enl. rev. edn (in Russian). Nedra, Moscow

Neukum G, Jaumann R, Hoffmann H, Hauber E, Head JW, Basilevsky AT, Ivanov BA, Werner SC, van Gasselt S, Murray JB, McCord T, the HRSC Co-Investigator Team (2004) Recent and episodic volcanic and glacial activity on Mars revealed by the High Resolution Stereo Camera. Nature 432:971–979

Nimmo F, Pappalardo RT, Giese B (2003) On the origins of band topography, Europa. Icarus 166:21–32

Nozette S, Rustan P, Pleasance LP, Horan DM, Regeon P, Shoemaker EM, Spudis PD, Acton CH, Baker DN, Blamont JE, Buratti BJ, Corson MP, Davies ME, Duxbury TC, Eliason EM, Jakosky BM, Kordas JF, Lewis IT, Lichtenberg CL, Lucey PG, Malaret E, Massie MA, Resnick JH, Rollins CJ, Park HS, McEwen AS, Priest RE, Pieters CM, Reisse RA, Robinson MS, Smith DE, Sorenson TC, Vorder Breugge RW, Zuber MT (1994) The Clementine mission to the Moon: scientific overview. Science 266:1835–1839

Nyrtsov MV (2000) Developing map projections of actual surfaces of celestial bodies and methods of their study. Abstract of Ph.D. thesis (in Russian). Moscow State University of Geodesy and Cartography, Moscow

O'Leary DW, Friedman JD, Pohn HA (1976) Lineament, linear, lineation: some proposed new standards for old terms. Geol Soc Amer Bull 87:1463–1469

Quinn P, Beven K, Lamb R (1995) The ln(a/tan β) index: how to calculate it and how to use it within the TOPMODEL framework. Hydrol Proc 9:161–182

Rappaport NJ, Konopliv AS, Kucinskas AB, Ford PG (1999) An improved 360 degree and order model of Venus topography. Icarus 139:19–31

Sadovnichy VA, Serbenyuk SN, Belov VP, Komissarov VV, Musin OR, Novakovsky BA, Sytenko IN, Usikov DA (1991) Digital model of Phobos surface (in Russian, with English abstract). Vest Mosc Univ, Geogr Ser 2:43–54

Saunders RS, Pettengill GH (1991) Magellan: mission summary. Science 252:247–249

Scott DH, Carr MH (1978) Geologic map of Mars, I-1083. Scale 1:25,000,000. US Geological Survey, Reston

Seidelmann PK, Abalakin VK, Burša M, Davies ME, de Bergh C, Lieske JH, Oberst J, Simon JL, Standish EM, Stooke P, Thomas PC (2002) Report of the IAU/IAG Working Group on cartographic coordinates and rotational elements of the planets and satellites: 2000. Cel Mech Dyn Astr 82:83–111

Shary PA (1995) Land surface in gravity points classification by complete system of curvatures. Math Geol 27:373–390

Shary PA, Sharaya LS, Mitusov AV (2002) Fundamental quantitative methods of land surface analysis. Geoderma 107:1–32

Shults SS (1970) Lineaments (in Russian). Vest Leningr Univ, Geol Geogr Ser 24:50–56

Simons M, Hager BH, Solomon SC (1994) Global variations in the geoid/topography admittance of Venus. Science 264:798–803

Sjogren WL (1997) Magellan spherical harmonic and gravity map data V1.0, MGN-V-RSS-5-GRAVITY-L2-V1.0, NASA planetary data system, http://pds-geosciences.wustl.edu/missions/magellan/shadr_topo_grav/index.htm

Slyuta EN, Kudrin LV, Sinilo VP (1989) Preliminary data on the nature of a planetary system of lineaments observed in radar images of Venus (data from Venera-15 and -16). Cosmic Res 27:786–797

Smith DE (2003) MGS MOLA mission experiment gridded data record, MGS-M-MOLA-5-MEGDR-L3-V1.0, NASA planetary data system, http://pds-geosciences.wustl.edu/missions/mgs/megdr.html

Smith DE, Zuber MT, Neumann GA, Lemoine FG (1997) Topography of the Moon from the Clementine lidar. J Geophys Res E102:1591–1611

Smith DE, Sjogren WL, Tyler GL, Balmino G, Lemoine FG (1999) The gravity field of Mars: results from Mars Global Surveyor. Science 286:94–97

Smith DE, Zuber MT, Solomon SC, Phillips RJ, Head JW, Garvin JB, Banerdt WB, Muhleman DO, Pettengill GH, Neumann GA, Lemoine FG, Abshire JB, Aharonson O, Brown CD, Hauck SA, Ivanov AB, McGovern PJ, Zwally HJ, Duxbury TC (1999) The global topography of Mars and implications for surface evolution. Science 284:1495–1503

Solomon SC, Head JW, Kaula WM, McKenzie D, Parsons B, Phillips RJ, Schubert G, Talwani M (1991) Venus tectonics: initial analysis from Magellan. Science 252:297–312

Speight JG (1974) A parametric approach to landform regions. In: Brown EH, Waters RS (eds) Progress in geomorphology: papers in honour of DL Linton. Institute of British Geographers, London, pp 213–230

Stepinski TF, Stepinski AP (2005) Morphology of drainage basins as an indicator of climate on early Mars. J Geophys Res 110:E12S12

Swets JA (1961) Detection theory and psychophysics: a review. Psychometrika 26:49–63

Takahashi H (1981) A lineament enhancement technique for active fault analysis In: Machine processing of remotely sensed data with special emphasis on range, forest, and wetlands assessment. Proc 7th Int Symp, June 23-26, 1981. Purdue University, West Lafayette, pp 103–112

Tokano T (2005) Water cycle in the atmosphere and shallow subsurface. In: Tokano T (ed) Water on Mars and life. Springer, Berlin, pp 191–216

Trifonov VG, Makarov VI, Safonov YG, Florensky PV (eds) (1983) Space remote-sensing data in geology (in Russian, with English contents). Nauka, Moscow

US Geological Survey (1972) Geologic atlas of the Moon. Scale 1:1,000,000. US Geological Survey, Washington

Vincenty T (1975) Direct and inverse solutions of geodesics on the ellipsoid with application of nested equations. Surv Rev 23:88–93

Watters TR, Cook AC, Robinson MS (2001) Large-scale lobate scarps in the southern hemisphere of Mercury. Plan Space Sci 49:1523–1530

Weijermars R (1985/86) The polar spirals of Mars may be due to glacier surges deflected by Coriolis forces. Earth Plan Sci Let 76:227–240

Wieczorek MA (2007) Gravity and topography of the terrestrial planets. In: Spohn T (ed) Treatise on geophysics, vol 10. Elsevier, Amsterdam, pp 165–206

Williams DA, Greeley R, Hauber E, Gwinner K, Neukum G (2005) Erosion by flowing Martian lava: New insights for Hecates Tholus from Mars Express and MER data. J Geophys Res 110:E05006

Wilson JP, Gallant JC (2000) Digital terrain analysis. In: Wilson JP, Gallant JC (eds) Terrain analysis: principles and applications. Wiley, New York, pp 1–28

Zlatopolsky AA (1992) Program LESSA (lineament extraction and stripe statistical analysis): automated linear image features analysis – experimental results. Comp Geosci 18:1121–1126.

Zuber MT (1996) Clementine lunar topography V1.0, CLEM1-L-LIDAR-5-TOPO-V1.0. NASA planetary data system, http://pds-geosciences.wustl.edu/missions/clementine/gravtopo.html

Zuber M, Smith DE, Lemoine FG, Neumann G (1994) The shape and internal structure of the Moon from the Clementine mission. Science 266:1839–1843

Zuber MT, Solomon SC, Phillips RJ, Smith DE, Tyler GL, Aharonson O, Balmino G, Banerdt WB, Head JW, Johnson CL, Lemoine FG, McGovern PJ, Neumann GA, Rowlands DD, Zhong S (2000) Internal structure and early thermal evolution of Mars from Mars Global Surveyor topography and gravity. Science 287:1788–1793